Ergodic-nonergodic phase diagram for a concentrated suspension of charge-stabilized colloids: Rescaled mean spherical approximation

S. K. Lai[1,2] and G. F. Wang[1]
[1]*Department of Physics, National Central University, Chung-li 320, Taiwan, Republic of China*
[2]*Department of Applied Physics, Royal Melbourne Institute of Technology, Melbourne, Victoria 3001, Australia*
(Received 10 February 1998)

We calculate the static structure factor of a concentrated suspension of charge-stabilized colloids using the mean spherical approximation, and apply the results obtained to determine its dynamical liquid-glass transition phase boundary within the idealized mode-coupling theory. It is found that the mean spherical approximation closure may yield an unphysical pair correlation function at the minimum distance of contact even at a high volume fraction ($\gtrsim 0.2$) when the coupling strength of charged colloids has attained certain high values. In addition, we notice that the Debye-Hückel screening constant κ defined parametrically in one component model generally differs from that defined in the primitive model. In other words, for a fixed macroion size, the κ employed in one-component model calculation may be physically unrealistic. Therefore, we rescale the static structure factor and impose the charge neutrality condition to achieve a self-consistent κ value for the one-component model and the primitive model. As a consequence, we are led to a reasonably reliable ergodic-nonergodic transition boundary that is applicable to charged colloids having different size and charge distribution. We confine our study to a monodisperse system and employ the effective screened Coulomb potential of Belloni [J. Chem. Phys. **85**, 519 (1986)] and of Derjaguin-Landau-Verwey-Overbeek to describe in parallel the interactions between colloidal particles. Since the screened Coulomb potential can be modeled to describe a wide range of interactions and has a universal dynamical phase transition loci, our present analysis therefore provides a practical means for extensive studies of charged colloidal structures and, within the mode-coupling theory, of the dynamics of very high density colloids. [S1063-651X(98)14208-3]

PACS number(s): 61.20.Gy, 82.70.Dd, 64.70.Dv

I. INTRODUCTION

The occurrence in a supercooled or supercompressed liquid of a dynamical crossover μ_c (which is the temperature for quenching or density for supercompressing) lying well above the calorimetric glass transition point has been a subject of current experimental and theoretical interest. Such a crossover μ_c has been analyzed both in light scattering [1,2] and in neutron scattering [3] experiments, although a consistent interpretation of the observed dynamic data remains controversial [4]. Theoretically the existence of μ_c was first predicted in 1984 by Bengtzelius, Götze, and Sjölander [5] who generalized the Boltzmann collision theory for short-range hard-core interactions and the Vlasov plasma theory for long-range Coulombic interactions to include the cage-diffusive and Feynman back flow effects. This so-called mode-coupling theory (MCT) was originally developed for the study of supercooled simple monatomic liquids. The MCT, however, was not given much attention at the time it was proposed, but the theory has been ever since in much dispute [6–8]. Recently there has appeared an increased interest in the MCT [9] due mainly to the possibility of comparing with experiments its several predictions such as the ergodic-nonergodic dynamical transition at μ_c, the square-root temperature dependence near μ_c, the spatial-temporal separation of the density-density correlation function near μ_c (the β-relaxation process) etc. Already the idealized glass-transition version of the MCT has been applied to the neutral hard spheres [10,11], charged hard spheres [12], Lennard-Jones atoms [13,14], pure liquid metals [15–17] as well as to slightly more complicated systems, which include the two-component charged hard spheres [18], two-component Lennard-Jones particles [19], binary neutral hard spheres [20], and molecular liquids [21–23]. These studies, though still somewhat simplified to be realized experimentally, are nonetheless quite instructive since the microscopic interactions that characterize these varied systems provide much physical insight for an understanding of the supercooled liquid dynamics. For instance, a comparison of the μ_c of neutral and charged hard-sphere systems [12] brings to light the subtle fine balance between the geometrical hard-core and long-range Coulombic influences on the dynamics of supercooled liquids and hence permits a plausible exploration of the cage-diffusive effect, which MCT believes to be the mechanism for the liquid-glass transition phenomenon. In our desire for a broad general study of the dynamics of liquids within the framework of MCT, we shall apply the technique of MCT to a study of the ergodic-nonergodic phase diagram for a charge-stabilized colloidal dispersion [24] since its static fluid structure, which is the sole input to MCT, can be calculated reliably and is available to experimental evaluation in addition to the theoretical verification of its universality [25–28].

A charge-stabilized colloidal dispersion such as a polyelectrolyte solution of micelles, or perhaps proteins, etc., is composed of highly charged macroions and singly or doubly charged small ions immersed in a solvent. This multicomponent system exhibits rather complex and generally nonlocal interparticle interactions, which have their physical origin arising from the high asymmetries of the size and charge of particles. Over the last fifteen years, statistical-mechanical

theories have played a key role both in uncovering these varied interactions and in enriching our knowledge of the intimately associated thermodynamical and structural properties. In the case of a fluid static structure factor $S(q)$ of a colloidal suspension, which is of direct relevance to our present work, there was major and significant theoretical development between the mid and late 1980s.

The simplest description for the $S(q)$ of colloids assumes the large finite-sized macroions (denoted by subscript 0 hereafter) as dominant charged particles and treats the pointlike small ions (indexed by 1 for counterions and by 2,3,... for co-ions below) and solvent as a uniform neutralizing background and both of these latter entities appear as screening constants in the electrostatic potential for macroions. This well-known one-component Derjaguin-Landau-Verwey-Overbeek (DLVO) [29] model gives an effective pair potential between macroions

$$\beta\phi_{00}(r)=\begin{cases}\infty, & r<\sigma_0\\ \dfrac{\overline{Z_0}^2\Lambda^2 L_B e^{-\kappa r}}{r}=\dfrac{\sigma_0\overline{\gamma}e^{-\kappa r}}{r}, & r>\sigma_0,\end{cases}\quad(1)$$

where the Bjerrum length $L_B=e^2\beta/(4\pi\epsilon\epsilon_0)$, $\beta=1/(k_BT)$ and ϵ are the inverse temperature and dielectric constant of the solvent, respectively; σ_0 ($\overline{Z_0}$) is the diameter (charge) of a macroion; $\kappa=(4\pi L_B\Sigma_{i=1}\rho_i Z_i^2)^{1/2}$ is the Debye-Hückel inverse screening length in which ρ_i and Z_i are respectively the number density and charge for small ions; $\Lambda\equiv\Lambda_{\mathrm{DLVO}}=\exp(\mathbf{k}/2)/(1+\mathbf{k}/2)$ where $\mathbf{k}=\kappa\sigma_0$ and finally for convenience in the following discussion we introduce the surface charge parameter $\overline{\gamma}=\beta\overline{Z_0}^2/[\pi\epsilon\epsilon_0\sigma_0(2+\mathbf{k})^2]e^{\mathbf{k}}$. Note that Eq. (1) for $\Lambda\equiv\Lambda_{\mathrm{DLVO}}$ was derived by the linearized Debye-Hückel equation [29] under the assumptions of low macroion number density $\rho_0\to 0$ and of weak coupling between small ions and macroions. In the usual DLVO form the ionic strength excludes contribution from the colloid species. In other words Eq. (1) does not depend on the macroion volume fraction $\eta=\pi\sigma_0^3\rho_0/6$. However, here we have adopted a slightly different κ, which includes the counterions' contribution to the screening length. The same interparticle potential $\phi_{00}(r)$ was obtained by Grimson and Silbert [30] who applied the techniques of the pseudopotential theory and perturbation method previously used in the study of the thermodynamics of liquid metals, and independently by Löwen, Hansen, and Madden [31] who employed the well-known density-functional theory to quantitatively extract $\phi_{00}(r)$ from the free energy minimum. The latter work has in addition outlined the steps that should be taken if one were to go beyond the linear approximation.

Despite its qualitative feature, the DLVO one-component model (to be abbreviated as OCM hereafter) has been widely used in the literature to interpret the $S(q)$ of charged stabilized colloids obtained from either light scattering or neutron diffraction experiments. The main reason for its popularity can be attributed to two important works of Hayter *et al.* [32,33] who successfully derived an analytical $S(q)$ from $\phi_{00}(r)$ within the mean spherical approximation (MSA), and demonstrated its applicability by applying the derived $S(q)$ to study the structures of micellar dispersions [34]. In spite of its apparent success, the OCM has, however, been questioned for some non-negligible colloidal features missing in the theory. Questions such as the finite size of counterions (co-ions), which would lead to important effects on correlations between macroions, the low-density ρ_0 limit, which casts doubt on its validity at high colloidal concentrations, the dependence of $\phi_{00}(r)$ on η, etc., were raised in the literature. In an attempt to remedy these apparent drawbacks Medina-Noyola and McQuarrie [35] compared the $\phi_{00}(r)$ in the OCM with that in the original primitive model, which is a model solution with macroions and small ions treated on an equal footing. Within the MSA, they showed that the $\phi_{00}(r)$ of OCM can be deduced *exactly* from the primitive model and, with further analysis, they succeeded in deriving an explicit expression for the $\phi_{00}(r)$ of two interacting colloidal particles embedded in a solution of finite-sized ions. In a separate work, Medina-Noyola [36] extended the same approach to the case of a salt-free suspension at any finite colloidal concentration but confined his analysis to the ''dense point limit'' by taking $Z_i/Z_0\to 0$. A theoretically more appealing work was reported by Beresford-Smith, Chan, and Michell [37,38] who applied the prescription of McMillan and Mayer [39] to construct an *effective* one-component direct correlation function $\hat{c}^{\mathrm{eff}}(q)$ [defined by $\hat{c}^{\mathrm{eff}}(q)=[1-1/S(q)]/\rho_0$] from an asymmetric multicomponent electrolyte system. Specifically they proposed a ''jellium'' approximation, which is a simplifying means to describe the correlation between a tagged colloidal particle and a small ion carried out by ignoring at the same time correlations among the remaining colloidal particles. For colloidal particles, they obtained a $\phi_{00}(r)$ with the coefficient $\Lambda=\Lambda_{\mathrm{DLVO}}(1+\eta)$. Further analysis on the highly charged effect of colloids led them to an *asymptotic* form of $\phi_{00}(r)$ having the same Yukawa behavior but with a Λ that has to be determined numerically by solving a differential equation. This ''jellium'' approximation was improved in the following year by Belloni [40] by replacing the jellium approximation for macroions with its discrete counterparts and in this environment accounted for the macroion–small-ion correlations using the analytical results of Hiroike [41]. For point ions, he succeeded in ''identifying'' naturally a one-component Yukawa form for $\phi_{00}(r)$ and derived an analytically *exact* expression for the coupling strength Λ. His numerical $S(q)$ results indicated clearly the equivalence between the primitive model and OCM under certain colloidal conditions (such as for pointlike small ions, significantly large asymmetry in sizes of macroions and ions, etc.). Concurrently, inspired by the latter work and motivated by their need for an analytical $S(q)$ for interpreting measured $S(q)$, Chen *et al.* [42] revisited this problem of the equivalence between the OCM and primitive model within MSA; they pointed out that the $\phi_{00}(r)$ given by Belloni is in fact, as in the dilute limit of the DLVO theory, the effective direct correlation function $\hat{c}^{\mathrm{eff}}(q)$ of colloidal particles without necessity to invoke the MSA closure. Accordingly they analyzed the mathematical structure of the screened Coulomb potential $\phi_{00}(r)$ and exploited the factor $\overline{Z_0}\Lambda$ appearing in Eq. (1) fully. This so-called generalized OCM has thus been used by them to interpret the observed $S(q)$ of proteins in place of the usual DLVO theory. In subsequent development, different efforts that aim at more general studies of colloidal systems were reported. These included focusing on the multicomponent nature of colloidal

systems [43], reexamining quantitatively the effect of high Z_0 for macroions and its related consequences on the nonadditivity radii of macroion–small-ion correlation [44], incorporating larger η and finite size of small ions [45,46], testing various closures [47], simplifying solutions for Yukawa mixtures with factorized coupling constants [48,43], exploring the physical roots for the analytical solutions [49,50], etc. Despite these endeavors, it would be, however, noteworthy to mention two earlier works. The first one is the study of $S(q)$ by Ronis [51] who applied a mixture of hard spheres in combination with the Gibbs-Bogoliubov inequality to a system of highly charged colloids at a low ionic strength. Using the Percus-Yevick hard-spheres mixture as a reference system, he determined the best hard-sphere diameters that mimic a suspension of charge-stabilized particles. For the case of additive diameters, he was able to account for the experimental $S(q)$; his approach failed for the more realistic case of nonadditive diameters. The second one, which was mentioned above, is a similar calculation by Khan *et al.* [44] who derived an analytical Yukawa potential for an effective OCM for macroions. The most important aspect of this work is that the nonadditive property for the macroion–small-ion correlation is explicitly included and was shown by the authors to yield a reasonably good description for $S(q)$. It appears that this $S(q)$ theory of Khan *et al.* is quite successful for studying the $S(q)$ of the highly charged colloids and micellar solutions at low η; it is not clear if the theory works well for cases of high volume fractions. Nonetheless, both these calculations clearly point to the importance of macroion–small-ion correlations in the study of colloid-colloid structure. In more recent years, statistical-mechanical studies of the $S(q)$ of charge-stabilized colloids have not progressed very far from the above brief review. There are more refined works reported that deal with high asymmetries of particles in both size and charge (for a more recent work see [52]). These calculations generalize or modify the same techniques as described above.

Among all these previous and recent works it appears to us that the work by Belloni [40] contains the essential physics of a concentrated suspension of charge-stabilized particles whose $S(q)$ is needed for our present study of the phase diagram of the liquid-glass transition. In this paper we thus apply the OCM of Belloni and use the analytical solution of Hayter and Penfold [32] to construct the corresponding OCM $S(q)$. As demonstrated below, there is an apparent inconsistency in the Debye-Hückel screening constant when the latter is used as a structural parameter in the OCM $S(q)$. This inconsistency, however, can be removed by renormalizing the macroion charge and size subject to the condition of charge neutralization. Once this is done, the physical parameters in the OCM $S(q)$ are seen to correspond to the associated colloidal parameters in the more general case of the primitive model [46]. Accordingly, one can easily prepare a $S(q)$ under specific colloidal conditions and yet retain the simple picture of OCM. Differing from previously published works, our study of the liquid-glass transition brings us to the regime of concentrated colloids at both a high volume fraction $\eta(\gtrsim 0.2)$ and a large macroion charge. Contrary to one's anticipation, we find that, for finite $\eta \lesssim 0.43$, and depending on the strength of the Coulomb repulsion, the MSA for the pair correlation function may become unphysical near the contact distance and thus needs to be remedied by a rescaling procedure [33,45,46,40]. In this work we compare the ergodic-nonergodic phase boundaries in the DLVO and Belloni models determined by the idealized MCT for $S(q)$ with and without rescaling. Although it is not the main purpose of this work we note that once the phase diagram is determined, one can calculate readily the mode-coupling temporal parameter from which other exponent parameters follow straightforwardly. The dynamical phenomena of a supercompressed suspension of charge-stabilized colloidal particles near μ_c can accordingly be investigated within the MCT.

II. THEORY

A. Mean spherical approximation

In this section we present the MSA for the $S(q)$ of charge-stabilized colloidal suspensions. For point ions, the $S(q)$ is analytically available and in conjunction with the idealized MCT will be used to locate the ergodic-nonergodic transition loci. The dynamics of the supercompressed phase comes as a corollary. For convenience in the following discussion, we give a brief summary of essential equations that lead to $\phi_{00}(r)$ following mainly several recent works [37–40]. In addition, we introduce in the Appendix the method of convolution, which may be useful in other contexts.

In the primitive model, one begins with a set of coupled multicomponent Ornstein-Zernike equations given by

$$h_{ij}(r) = c_{ij}(r) + \sum_{l=0} \rho_l \int h_{il}(|\mathbf{r}-\mathbf{r}'|) c_{lj}(r') d\mathbf{r}', \quad (2)$$

where i, j, and l refer to different species: $i,j,l=0$ for maroions, $i,j,l=1$ for counterions, and $i,j,l=2,3,...$ for coions. Here ρ_l is the number density for species l; $c_{ij}(r)$ is the direct correlation function and $h_{ij}(r)=g_{ij}(r)-1$, defined in terms of the pair correlation function $g_{ij}(r)$, is the total correlation function. Thus, the primitive model is by construction a mixture of charged hard spheres characterized by different diameters. In the effective direct correlation function approach, one can show formally [39] that Eq. (2) can be contracted to an effective direct correlation function $c_{00}^{\mathrm{eff}}(r)$, which satisfies

$$h_{00}(r) = c_{00}^{\mathrm{eff}}(r) + \rho_0 \int h_{00}(|\mathbf{r}-\mathbf{r}'|) c_{00}^{\mathrm{eff}}(r') d\mathbf{r}', \quad (3)$$

where, in the Fourier-transformed space, $c_{00}^{\mathrm{eff}}(q)$ can be written as

$$\hat{c}_{00}^{\mathrm{eff}}(q) = \hat{c}_{00}(q) + \hat{\mathbf{c}}_0^{\mathbf{T}} \cdot [\mathbf{1} - \hat{\mathbf{c}}^*]^{-1} \cdot \hat{\mathbf{c}}_0. \quad (4)$$

In Eq. (4) $\hat{\mathbf{c}}_0$ is a column matrix defined by

$$(\hat{\mathbf{c}}_0)_i = \rho_i^{1/2} \hat{\mathbf{c}}_{0i}(q), \quad i=1,2,\ldots, \quad (5)$$

which describes the macroion–small-ion correlations, **1** is a matrix, and $\hat{\mathbf{c}}^*$ is a matrix giving the small-ion–small-ion correlations, viz.,

$$(\hat{\mathbf{c}}^*)_{ij} = \rho_i^{1/2} \rho_j^{1/2} \hat{\mathbf{c}}_{ij}(q), \quad i,j=1,2,\ldots. \quad (6)$$

For pointlike ions, the direct correlation function $c_{ij}(r)$, $i,j=0,1,2,...$ can be written in terms of the short-range $c_{ij}^{s}(r)$ as [41]

$$c_{ij}(r)=c_{ij}^{s}(r)-\frac{Z_iZ_jL_B}{r},\quad r>0 \tag{7}$$

where $c_{00}^{s}(r)=0$ for $r>\sigma_0$, and

$$c_{ij}^{s}(r)=0\quad (i,j=1,2,\dots)\quad r>0, \tag{8}$$

$$c_{0i}^{s}(r)=0\quad (i=1,2,\dots)\quad r>\sigma_0/2. \tag{9}$$

If we take the Fourier transform of Eqs. (8) and (9), apply them to Eqs. (5) and (6), and substitute the results into Eq. (4), we obtain

$$\hat{c}_{00}^{\rm eff}(q)=\hat{c}_{00}^{s}(q)+\sum_{i=1}[c_{0i}^{s}(q)]^2-\frac{[\alpha_0+\Sigma_{i=1}\alpha_i c_{0i}^{s}(q)]^2}{q^2+\kappa^2}. \tag{10}$$

Here, $\alpha_i^2=4\pi L_B\rho_i Z_i^2$ and $\kappa=(\Sigma_{i=1}\alpha_i^2)^{1/2}$. Next, we perform the inverse Fourier transform of Eq. (10); the first and second terms vanish identically for $r>\sigma_0$ while for the third terms they can be convoluted (see Appendix for details) to yield

$$c_{00}^{\rm eff}(r)=-Z_0^2L_BX^2\frac{e^{-\kappa r}}{r},\quad r>\sigma_0, \tag{11}$$

where

$$X=\cosh\left(\frac{\mathbf{k}}{2}\right)+U\left[\frac{\mathbf{k}}{2}\cosh\left(\frac{\mathbf{k}}{2}\right)-\sinh\left(\frac{\mathbf{k}}{2}\right)\right] \tag{12}$$

in which

$$U=\frac{8\delta}{\mathbf{k}^3}-\frac{2\nu}{\mathbf{k}}, \tag{13}$$

with

$$\delta=\frac{3\eta}{1-\eta}, \tag{14}$$

$$\nu=\frac{\Gamma\sigma_0/2+\delta}{1+\Gamma\sigma_0/2+\delta}, \tag{15}$$

and

$$\Gamma^2=\kappa^2+\frac{\alpha_0^2}{(1+\Gamma\sigma_0/2+\delta)^2}. \tag{16}$$

Given Z_0, σ_0, $\mathbf{k}$, and η, Eq. (16) has to be solved iteratively for Γ and hence X in Eq. (12). It is interesting to note that $X\to\Lambda_{\rm DLVO}$ in the limit $\rho_0\to 0$. On the other hand, for a given X, Eq. (11) is similar in form to Eq. (1) and as was pointed out by Chen *et al.* [42] Eq. (11) resembles the MSA closure

$$g_{ij}(r)=0,\quad r<\sigma_{ij}, \tag{17}$$

$$c_{ij}(r)=-\beta\phi_{ij}(r),\quad r>\sigma_{ij} \tag{18}$$

if one identifies the right-hand side of Eq. (11) to be an effective interparticle potential $\beta\phi_{00}^{\rm eff}(r)$ for macroparticles, and defines $\sigma_{0i}=\sigma_0/2$. This identification is natural, and practically, it is necessary and convenient since analytical solution [32,33] of $S(q)$ within MSA exists. Note that Eq. (18) in the form defined is customarily considered as a linearized closure relation, which is correct for a low charged system and becomes less reliable for polyelectrolyte systems at low concentration. It was, however, implicit in the works of Beresford-Smith *et al.* [37], Belloni [40], and Chen *et al.* [42] that, within the effective direct correlation function scheme, such basic assumptions can be relaxed. Thus the use of Eq. (11) does not necessarily imply a case for a polyelectrolyte system of low concentration since the needed $S(q)$ can be obtained by

$$S(q)\equiv S_{00}(q)=\frac{1}{[1-\rho_0\hat{c}_{00}^{\rm eff}(q)]}, \tag{19}$$

which is essentially a OCM.

B. Mode-coupling approximation for a colloidal dispersion

The MCT focuses on the time-dependent density-density correlation function defined by

$$F(q,t)=\langle\delta n(\mathbf{q},t)\,\delta n(-\mathbf{q},0)\rangle, \tag{20}$$

where $\delta n(\mathbf{q},t)$ is the Fourier transform of the microscopic density fluctuation $\delta n(\mathbf{r},t)$ and $\langle\ \rangle$ is the usual ensemble average. This function spatially contains useful information on the local structure of colloidal particles and temporally accounts for its time evolution. Defining the Laplace transform by $\hat{F}(q,z)=\int_0^\infty dt\,\exp[-zt]F(q,t)$ and neglecting hydrodynamic interactions, it can be shown [27,26,25] that $\tilde{F}(q,z)$ is related to a memory function $\hat{M}(q,z)$ by [53]

$$\hat{R}(q,z)\equiv\frac{\hat{F}(q,z)}{S(q)}=\frac{1}{z+\omega(q)[1-\hat{M}(q,z)/(q^2D_0)]}, \tag{21}$$

where $\omega(q)=q^2D_0/S(q)$ and D_0 is the Stokes-Einstein diffusion coefficient of a single particle. As discussed in [27], $F(q,t)$ consists of a short-time ($\tau_{\mathbf{I}}\gg t\gg\tau_{\mathbf{B}}$, where for typical aqueous colloidal suspensions $\tau_{\mathbf{B}}\approx 10^{-9}-10^{-8}$ s and $\tau_{\mathbf{I}}\approx 10^{-3}$ s) decaying component representing a Brownian-type motion and of a long-time ($t\gg\tau_{\mathbf{I}}$) slowly decaying part $\Pi(q,t)$ characterizing collective nonlinear couplings of the sluggish behavior of $F(q,t)$. It was pointed out, however, by Cichocki and Hess [26] that the memory function $\hat{M}(q,z)$ in Eq. (21) is not an elementary memory function in the study of dynamic properties of colloidal particles since its time evolution operator is not one-particle irreducible. By comparing the generalized dynamic viscosity obtained from a generalized Smoluchowski equation and a Fokker-Planck equation, they were able to derive a formally exact relation between $\hat{M}(q,z)$ and an irreducible collective memory function $\hat{\mathcal{M}}(q,z)$. Now, at high densities, the slowly decaying component $\hat{\mathcal{M}}(q,z)\approx\Pi(q,t)$ is manifestly dominant compared with the short-time contribution. In fact it can be inferred from the works of Szamel and Löwen [25], Baur *et al.*

[27], Kawasaki [28], and Bengtzelius *et al.* [5] that an idealized liquid-glass transition sets in at a dynamical transition point μ_c if there exists a solution $f_c(q)$ for the following nonlinear vitrification equation:

$$\frac{f(q)}{1-f(q)}=\frac{S(q)}{D_0q^2}\,\Pi(q,t=\infty)=\mathcal{F}_q(f(k)). \tag{22}$$

The $f_c(q)=R(q,t\to\infty)\neq 0$ is the Debye-Waller factor corresponding to the nonergodic state whereas $f(q)=0$ is the ergodic state. We note that $f(q)$ can be compared directly with experiment since it corresponds to the form factor for the elastic part of the coherent spectrum in neutron scattering experiments. This function also accounts for the nondiffusive states as the liquid phase approaches the glassy region. By making a two-mode approximation as in atomic liquid [54,5], the more fundamental long-time memory function $\Pi(q,t)$ can be derived to read [25,27]

$$\Pi(q,t)=\frac{D_0\rho_0}{8q\pi^2}\int_0^\infty dx\,x\int_{|x-q|}^{|x+q|}dy\,y\left(\frac{x^2-y^2}{2q}\,[c(x)-c(y)]+\frac{q}{2}\,[c(x)+c(y)]\right)^2 S(x)S(y)R(x,t)R(y,t), \tag{23}$$

where $c(q)$ is the direct correlation function. It should be emphasized that Eq. (23), which is derived for a colloidal suspension, has exactly the same form as that for an atomic liquid (cf. Eq. (19) [25] with Eq. (2.4) in [55]). Given $S(q)$, Eqs. (22) and (23) constitute the two coupled equations, which will be used below to locate the liquid-glass transition loci.

III. NUMERICAL RESULTS AND DISCUSSION

We now apply the effective direct correlation function $c_{00}^{\rm eff}(r)$, which is identified to be an effective potential $-\beta\phi_{00}^{\rm eff}(r)$ by Eq. (11). This defined potential encompasses a remarkably rich phase behavior with fluid structures exhibiting very short-ranged (characterized by the hard-core σ_0 or the volume fraction $\eta=\pi\sigma_0^3\rho_0/6$), intermediate-ranged (dictated by the screened Coulomb parameter $\mathbf{k}=\kappa\sigma_0$), and very long-ranged (described by the charge Z_0) interactions. Now in order to locate the ergodic-nonergodic transition loci by solving Eqs. (26) and (27) iteratively and self-consistently for $f_c(q)$, we need the fluid static structure factors of Eq. (11). Within the MSA for pointlike small ions the latter can formally be calculated from the primitive model whose structure factor was shown by Belloni [40] to be *exactly* the same as that in the OCM. The calculation, though theoretically straightforward when applied in conjunction with the MCT in deducing the parametric phase diagram, is, however, useful only for specific colloidal suspensions. In view of this we have resorted to a more general means by employing the OCM $S(q)$. Strategically, one starts first by applying the idealized MCT to determine the phase boundary of the OCM-type potential given by Eq. (1) whose static structure factor [32] is *uniquely* determined for properly scaled parameters $(\eta,\mathbf{k},\overline{\gamma})$. Then, from the determined $(\eta_c,\mathbf{k}_c\overline{\gamma_c})$, we examine the necessity of rescaling for macroions at contact following the recipe of Sheu *et al.* [56] and of Hansen and Hayter [33]; we deduce for pointlike ions the Z_0, σ_0, and associated quantities in the OCM of Belloni [40] under physically reasonable conditions.

A. $S(q)$ in rescaled mean spherical approximation

As pointed out in the Introduction, we will encounter a situation where the pair correlation function $g(r)$ may become unphysical at the minimum distance of contact $R=1^+$ where we define $R=r/\sigma_0$. This unpleasant feature arises from the inadequacy of MSA in accounting for the short-range correlation. To overcome this inherent deficiency, both the numerical method of Belloni [40] and Sheu *et al.* [56] and the analytical formula of Hansen and Hayter [33] were attempted. For the numerical means, we proceed as follows. First, the analytical $S(q)$ of Hansen and Hayter [33] at $(\eta,\mathbf{k},\overline{\gamma})$ is Fourier transformed to obtain the $g(r)$. If the macroions at contact are positive, i.e., $g(R=1^+)>0$, we accept the $S(q)$, otherwise we employ the rescaling technique by increasing η to $\eta'=\eta+\Delta\eta$ and accordingly $\mathbf{k}'=\mathbf{k}(\eta'/\eta)^{1/3}$ at the same coupling constant $\overline{\gamma}'=\overline{\gamma}(\eta/\eta')^{1/3}$. Next, the rescaled $S(q)$ is Fourier transformed again and $g(R=1^+)$ is examined. If it is negative, we repeat the procedure by increasing $\Delta\eta$. If, however, $g(R=1^+)>0$ we choose a smaller $\Delta\eta$ and repeat the numerical computation for $S(q)$. The calculation proceeds until the criterion $g(R=1^+)=0$ is achieved. It should be emphasized that this rescaling scheme automatically guarantees the coupling constant Λ in either the Belloni or DLVO model to remain unchanged. In other words, the rescaling only applies to the macroion-macroion correlation so that the potential $\phi_{00}^{\rm eff}(r)$ for distance greater than the rescaled size is unperturbed, and any macroion-ion correlation should not be perturbed during the renormalization. For the analytical means, we apply the formula

$$g_\eta(R=1^+)=-(p_1+p_2C+p_3F), \tag{24}$$

where p_i, C, and F are coefficients defined in terms of $(\eta,\mathbf{k},\overline{\gamma})$ [33]. The rescaling parameters $(\eta',\mathbf{k}',\overline{\gamma'})$ are defined as described above except that their values are determined by resorting to Eq. (24) and $g_{\eta'}(R=1^+)=0$. In all our calculations these two methods agree almost exactly. As a means to assess the present model, we depict in Fig. 1 our rescaled MSA (RMSA) $S(q)$ compared with that of the hypernetted-chain closure [57] and with that of Senatore [58] using the model of Khan *et al.* [44]. These results show that the present model of Belloni is as good a choice for $S(q)$ as the latter.

B. Ergodic-nonergodic phase diagram

To begin with we consider a concentrated suspension of charge-stabilized colloids described by parameters typically encountered in aqueous macroion solutions, namely, $T=298$ K, $\epsilon=78.3$, and $\sigma_0=5$ nm. Under these physical conditions, we start with the strong screening case $\mathbf{k}=6$ and for η in the range $0.55>\eta>0.15$ vary $\overline{\gamma}$ for selected η until nonergodic solutions are found. In the parametric space of $(\eta,\mathbf{k},\overline{\gamma})$ this procedure traces out the dynamical transition loci $\mu_c=(\eta_c,\mathbf{k}_c,\overline{\gamma_c})$ separating the ergodic regime $f(q)$

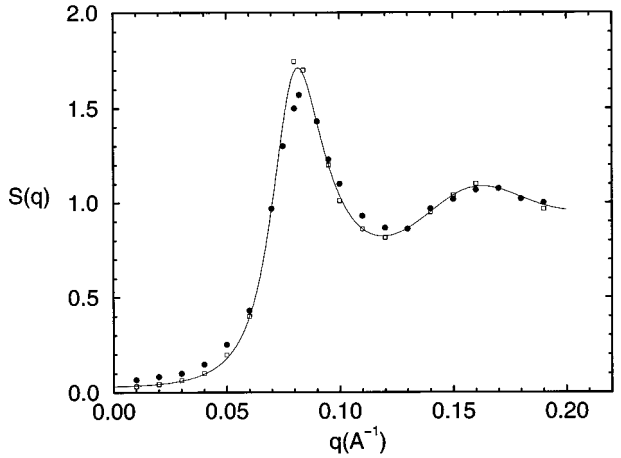

FIG. 1. Static structure factor $S(q)$ of a suspension of charge-stabilized colloids obtained using the method described in text (full curve) with the approximate treatment of the finite-size effect for counterions [40] compared with those calculated from hypernetted-chain closure [57] (open squares) and from RMSA model of Senatore [58] (closed circles). The latter two $S(q)$ are read directly from Fig. 2(b) of Ref. [58]. Parameters used are $\sigma_0/\sigma_1=50/5$ Å, $Z_0/Z_1=-40/1e$, and $\rho_0/\rho_1=2.5\times10^{-3}/100\times10^{-3}M$.

$=0$, $\eta-\overline{\gamma}<\eta_c-\overline{\gamma_c}$, from the nonergodic regime $f_c(q)\neq0$, $\eta-\overline{\gamma}\geqslant\eta_c-\overline{\gamma_c}$. The same numerical process was repeated for a weak screening case $\mathbf{k}=3$. Figures 2(a) and 2(b) show our results of computations for the above two cases. From these figures it was found, however, that $g(R=1^+)<0$ for $\eta_c\lesssim0.43$, which implies an inadequacy of $S(q)$, although Eqs. (22) and (23) less reliably predict a loci of nonergodic form factors. In view of this unsatisfactory drawback, we first apply the rescaling scheme to these $S(q)$ and check for each $(\eta,\mathbf{k},\overline{\gamma})$ the magnitude of the eigenvalue (equal to one at μ_c) to see what changes should be made to $\overline{\gamma}$. Then, at given $\mathbf{k}_c$ and η_c, we vary $\overline{\gamma}$ by $\overline{\gamma}+\overline{\Delta\gamma}$. This set of parameters $(\eta_c,\mathbf{k}_c,\overline{\gamma}+\overline{\Delta\gamma})$ are then subject to the rescaling process and $\overline{\gamma_c}$ is subsequently located by substituting the rescaled $S(q)$ at $(\eta',\mathbf{k}',\overline{\gamma}')$ into Eqs. (22) and (23). The $\overline{\gamma_c}$ thus calculated are displayed in the same Figs. 2(a) and 2(b). Note that for a Yukawa potential and for properly scaled parameters these two $\eta_c-\overline{\gamma_c}$ curves are *universal*. Thus, given $\mathbf{k}=3$ or 6, one may read from Figs. 2(a) and 2(b) the one-to-one correspondence between η_c and $\overline{\gamma_c}$.

At this point we should draw attention to an apparent inconsistency in both Figs. 2(a) and 2(b). The inconsistency lies in the use of fixed $\sigma_0=5$ nm, which, for any η_c, will yield a Debye-Hückel screening constant $\kappa=\mathbf{k}/\sigma_0$ that when evaluated at either $\mathbf{k}=3$ or 6 generally differs from the formula $\kappa=[4\pi L_B\Sigma_{i=1}\rho_i Z_i^2]^{1/2}$ (supplemented by the charge neutralization condition $\rho_0Z_0=\rho_1Z_1$). Such a difference in κ arises from the less quantitative nature of the OCM (notably for the DLVO approximation) and is implicit in several recent theoretical models proposed in the literature [59]. Physically this would imply that the value for the macroion size σ_0 and Z_0 needs readjustments in order to compensate for the difference in κ. Technically this can be accomplished by preparing for a list of $\sigma_0^{(j)}$ in the range $10\lesssim\sigma_0^{(j)}\lesssim6000$ Å the sequence of parameters $\rho_0^{(j)}=6\eta_c/(\pi\sigma_0^{(j)3})$, $\kappa^{(j)}=\mathbf{k}/\sigma_0^{(j)}$ and $Z_0^{(j)}$ (via $\kappa^{(j)}=[4\pi L_B\Sigma_{i=1}\rho_i Z_i^2]^{1/2}$ and $\rho_0^{(j)}Z_0^{(j)}=\rho_1Z_1$)

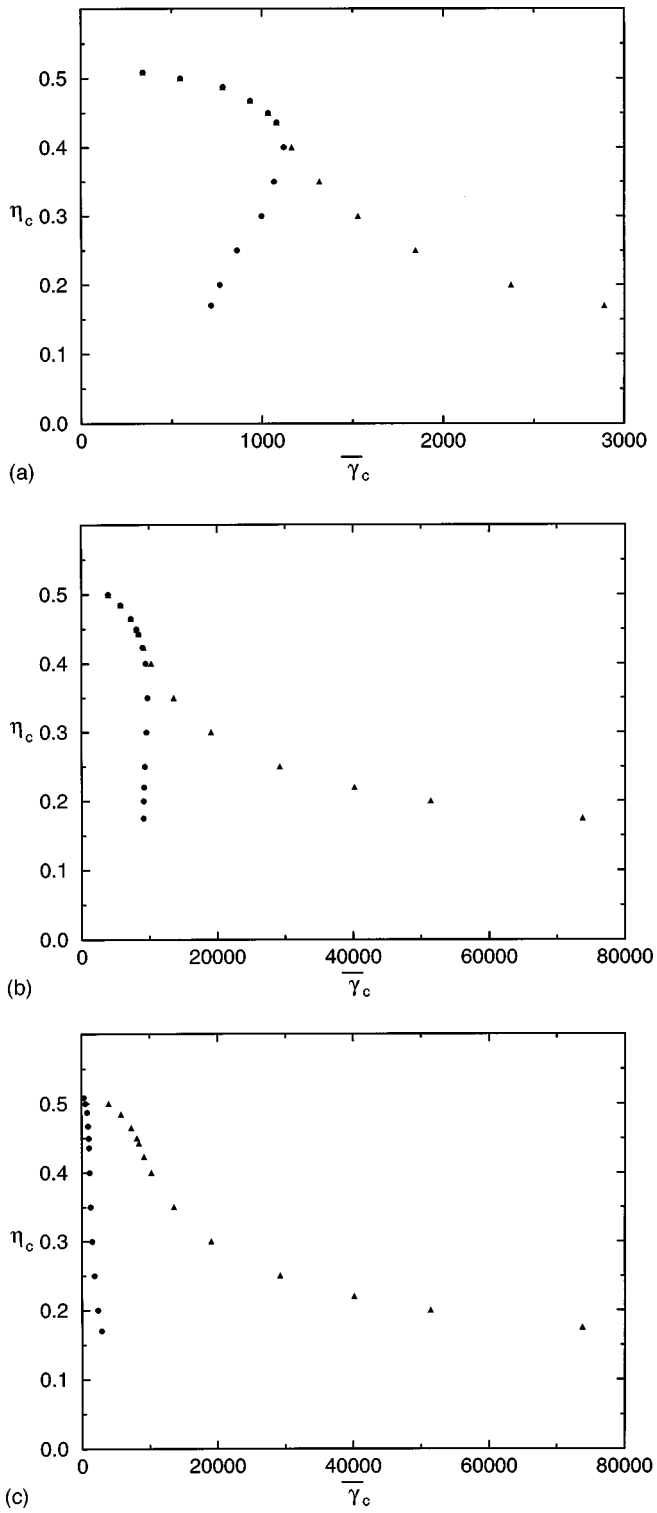

FIG. 2. (a) Volume fraction η_c vs surface charge parameter $\overline{\gamma_c}$ for screening parameter $\mathbf{k}=3$ in MSA (circles) and in RMSA (triangles). (b) Same as (a) but for $\mathbf{k}=6$. (c) Comparison of the loci of phase diagrams for $\mathbf{k}=3$ (circles) and $\mathbf{k}=6$ (triangles).

at $\mathbf{k}=3$ or 6, and for each selected η_c, these parameters are (a) substituted in the Belloni model into Eqs. (12)–(16) to solve iteratively for $X^{(j)}$ and (b) employed directly in the DLVO model to obtain Λ_{DLVO}. Next, we read from Fig. 2(a) or 2(b) the $\overline{\gamma_c}$ that corresponds to the specific η_c and in conjunction with the coupling strength $\overline{\gamma_c}$ of Eq. (11), i.e.,

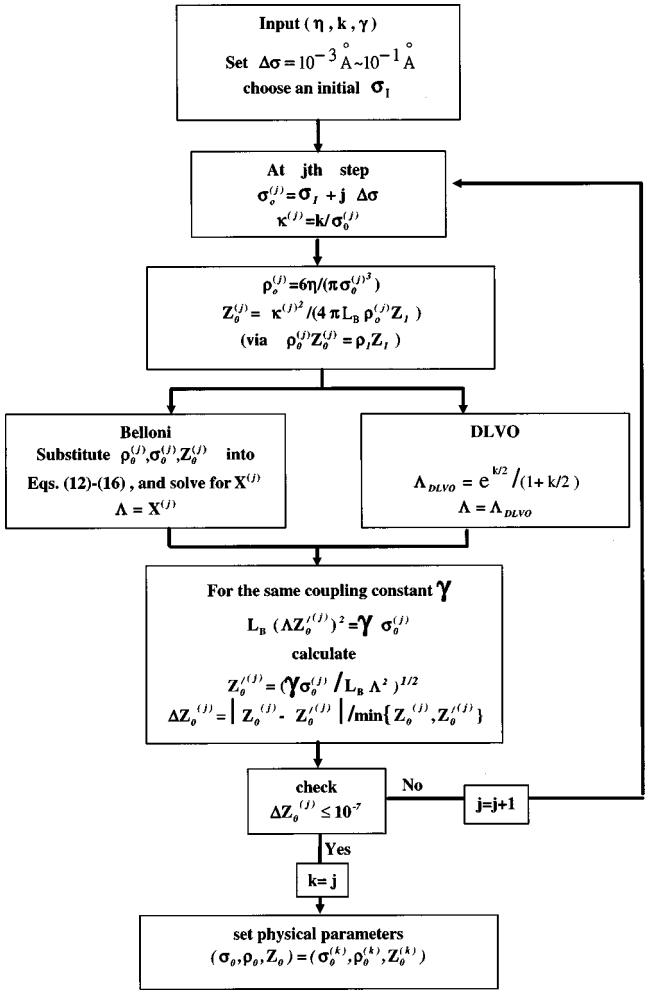

FIG. 3. Flow chart showing the procedure in achieving a self-consistent Debye-Hückel screening constant. Values of macroion charge and size for DLVO and Belloni models (see text) are adjusted to satisfy charge neutralization condition.

$Z_0^{(j)\prime 2}\Lambda^{(j)2}L_B=\sigma_0^{(j)}\overline{\gamma_c}$, extract the $Z_0^{(j)\prime}$. This $Z_0^{(j)\prime}$ is compared with the $Z_0^{(j)}$ and the whole procedure is repeated for each $\sigma_0^{(j)}$ in the list until the criterion $|Z_0^{(j)}-Z_0^{(j)\prime}|\leqslant 10^{-7}$ is achieved. Figure 3 is the flow chart dictating the details of the procedure. Note that, in the list-searching process, we consider only counterions (each with ionic charge $Z_1=1e$) for the ionic strength in κ, and the σ_0 is relaxed to ensure the phase diagram associated with the *same* coupling strength $\overline{\gamma_c}$.

We now comment on Figs. 2(a) and 2(b), which give the variation of η_c with $\overline{\gamma_c}$. We note two general features. First, for the two screening cases of interest here one notices quite substantial difference in the ergodic-nonergodic phase boundaries for the MSA with and without rescaling. For the MSA, after an initial decreasing tendency (for $0.51>\eta_c \gtrsim 0.43$), η_c changes abruptly for $\mathbf{k}=3$ and is almost η independent for $\mathbf{k}=6$. This behavior is in contrast to the RMSA where η_c decreases monotonously for the whole range of values $0.5>\eta_c\gtrsim 0.15$. Second, as Fig. 2(c) shows, the ergodic region for the strong screening case has an extensive region whereas in the weak screening case its domain is relatively more restrictive. The first general feature for the RMSA can be understood from two facets—the change in $\overline{\gamma_c}$

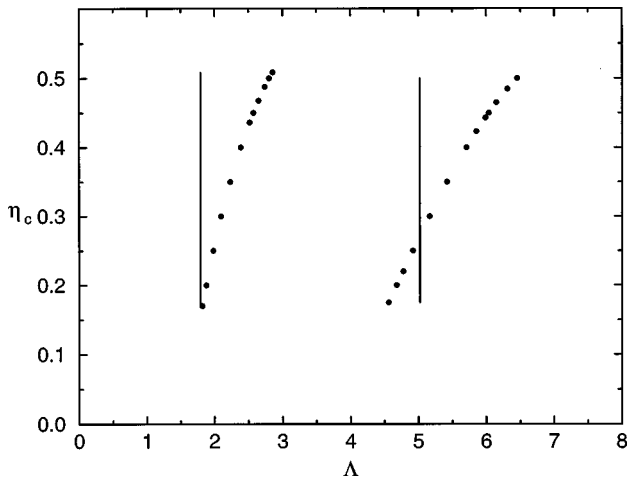

FIG. 4. Volume fraction η_c vs coupling parameter Λ [Eq. (1) in text] which is X (circles) in Belloni model and Λ_{DLVO} (full curves) in DLVO model for cases $\mathbf{k}=3$ (left curves) and $\mathbf{k}=6$ (right curves).

with $\mathbf{k}$ and with the macroion charge and σ_0^c. It would, however, be more instructive and concrete if these dependences were analyzed in terms of specific models, namely, $\sigma_0^c\overline{\gamma_c}=Z_0^{c2}X^2L_B$ for the Belloni model and $\sigma_0^c\overline{\gamma_c}=\overline{Z_0^{c2}}\Lambda_{\mathrm{DLVO}}^2L_B$ for the DLVO model. We show in Fig. 4 the change of η_c with X or Λ_{DLVO} at $\mathbf{k}=3$ and 6. There are distinct differences in these coupling constants—X decreases in magnitude and approaches Λ_{DLVO} as η_c decreases whereas Λ_{DLVO}, which is a function only of $\mathbf{k}$, is independent of η_c. To interpret the quantitative changes in the η_c-$\overline{\gamma_c}$ curves with $\mathbf{k}$ one needs, however, to consider the variation of η_c with the macroion charge as well as with σ_0^c. Figures 5 and 6 display the details of these structures. It is readily seen in Figs. 5(c) and 6 that at $\mathbf{k}=3$ although drastic differences are observed between the rescaled $\eta_c-Z_0^c$ ($\sigma_0^c-Z_0^c$) and $\eta_c-\overline{Z_0^c}$ ($\sigma_0^c-\overline{Z_0^c}$), the associated change of Z_0^{c2}/σ_0^c or $\overline{Z_0^{c2}}/\sigma_0^c$ (with η) on which $\overline{\gamma_c}$ is directly proportional does not vary greatly in *magnitude* for both OCM (see Fig. 7). On the other hand, Figs. 5(d) and 6 between the corresponding quantities at $\mathbf{k}=6$ differ much less severely but both the Belloni and DLVO models show a strong enhancement in *magnitude* of the Z_0^{c2}/σ_0^c or $\overline{Z_0^{c2}}/\sigma_0^c$ compared with the weak screening cases. These dependences thus account partly for the variation of η_c with $\overline{\gamma_c}$ in either the Belloni or DLVO model. As regards the second feature, it can be explained by the physical significance of $\mathbf{k}$, which is a screening parameter determined sensibly by the ionic strength of small ions now playing the role of charge stabilizing the macroparticles. Since the case $\mathbf{k}=6$ corresponds to a greater accumulation of ionic density for the Coulomb interactions between macroions to be effectively screened out, and that the above results for the X (Λ_{DLVO}) and Z_0^{c2}/σ_0^c ($\overline{Z_0^{c2}}/\sigma_0^c$) clearly point to a marked increase in magnitude of $\overline{\gamma_c}$ with $\mathbf{k}$, it is thus reasonable to see the strong screening case occupying a larger ergodic region.

To pursue our analysis further, we now scrutinize in greater detail Fig. 5(a) for the change of η_c with charge Z_0^c determined by $\overline{\gamma}=Z_0^2X^2L_B/\sigma_0$ and Fig. 5(b) for the change of η_c with charge $\overline{Z_0^c}$ deduced from $\overline{\gamma}=\overline{Z_0}^2\Lambda_{\mathrm{DLVO}}^2L_B/\sigma_0$. In

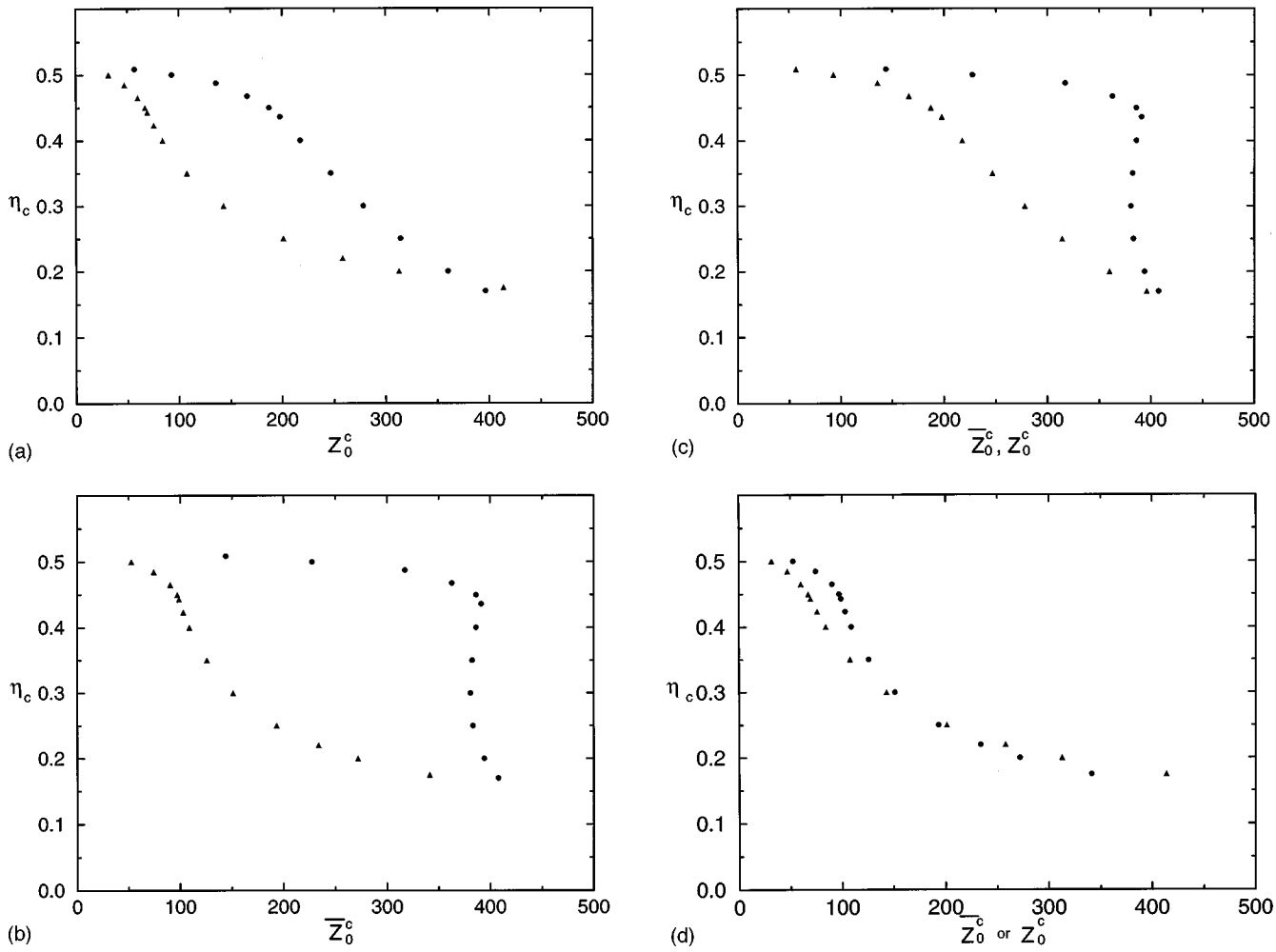

FIG. 5. (a) Volume fraction η_c vs macroion charge Z_0^c (in units of electronic charge) in the Belloni model for screening parameters $\mathbf{k}=3$ (circles) and $\mathbf{k}=6$ (triangles). (b) Same as (a) but for th e DLVO model. (c) Comparison of the volume fraction η_c vs macroion charge, Z_0^c for Belloni (triangles), and $\overline{Z_0^c}$ for DLVO (circles) models at $\mathbf{k}=3$. (d) Same as (c) but for $\mathbf{k}=6$.

addition, we examine also within the context of RMSA the relations $Z_0^c-\sigma_0^c$ and $\overline{Z_0^c}-\sigma_0^c$ given in Figs. 6(a) and 6(b). Two distinct aspects are observed.

(a) The RMSA results for η_c-Z_0^c curves in the Belloni model displayed in Fig. 5(a) for the strong and weak screening cases decrease monotonously and span over $56e \lesssim Z_0^c \lesssim 396e$ for $\mathbf{k}=3$ and $31e \lesssim Z_0^c \lesssim 414e$ for $\mathbf{k}=6$. In contrast, the corresponding η_c-$\overline{Z_0^c}$ curves in the DLVO model depicted in Fig. 5(b) for the strong screening case decreases monotonously while that for the case $\mathbf{k}=3$ it is virtually unchanged for $\eta_c \gtrsim 0.43$ and becomes nearly independent of η for $\eta_c < 0.43$. As a result the weak screening case $\mathbf{k}=3$ associated with the DLVO and Belloni models shows a marked difference in structures [Fig. 5(c)] compared with the strong screening cases [Fig. 5(d)].

(b) For each η_c-Z_0^c phase boundary given in Fig. 5(a) each dynamical transition point (η_c, Z_0^c) corresponds to a σ_0^c [Fig. 6(a)] determined as described in Fig. 3, while those of η_c-$\overline{Z_0^c}$ [Fig. 5(b)] the corresponding σ_0^c are given in Fig. 6(b). As can be seen easily the magnitude of σ_0 for $\mathbf{k}=3$ is significantly larger than the case $\mathbf{k}=6$.

The origin of the first aspect can be traced to the correlation between macroions and small ions, which was here exactly taken into account for pointlike ions through Eq. (10) and which has resulted in the strong dependence of η on Z_0^c (via the function X). For the case $\mathbf{k}=3$, ionic screening is comparatively less effective, which will thus increase the macroion charge Z_0^c. This ineffective screening effect is *further enhanced* by the strong dependence of X on η [in contrast to the DLVO model where $\Lambda_{\mathrm{DLVO}}=\exp(\mathbf{k}/2)/(1+\mathbf{k}/2)$], since the presence of other macroions has the consequence of decreasing the screening ability of small ions [40] (and hence increasing Z_0^c). Structural changes are therefore induced by a delicate balance between the hard-core repulsion and strong electrostatic coupling particularly near higher volume fractions. For the DLVO model, Λ_{DLVO} does not depend on η and thus has no relevance to $\overline{Z_0^c}$. The geometric hard-core factor in this weak screening case dominates the structure for $\eta_c \gtrsim 0.43$, but its role is taken over by the Coulomb repulsion for $\eta_c \lesssim 0.43$, which is found to be independent of η. On the other hand for the Belloni model X deviates from Λ_{DLVO} and has a robust dependence on η (and hence Z_0^c), which is manifested by an effective influence of the electrostatic coupling compared with the excluded volume effects. This explains the marked difference in behavior for the two weak screening cases given in Fig. 5(c). Never-

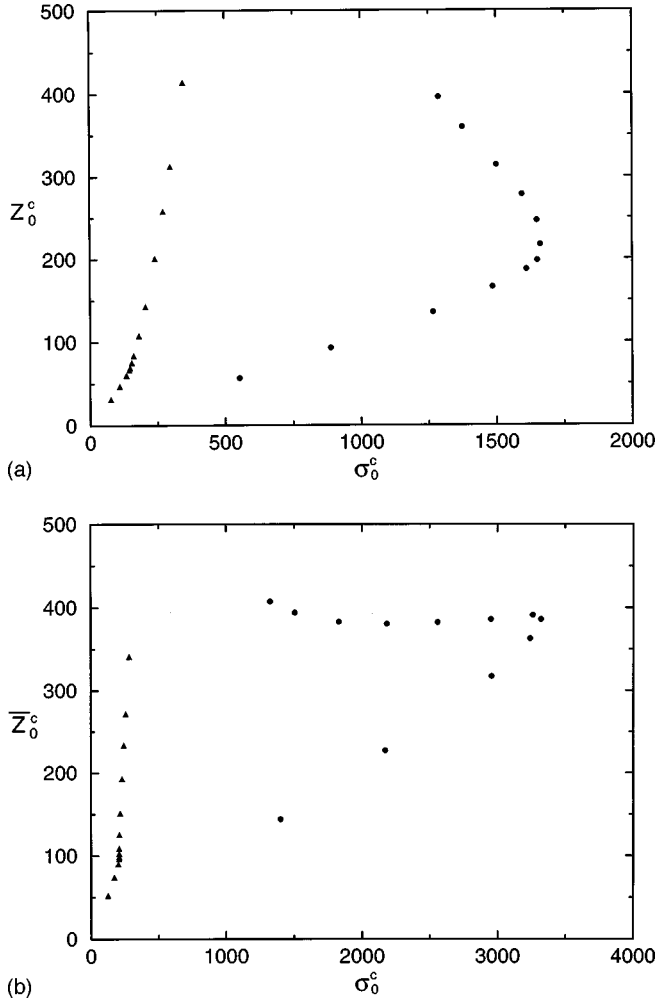

FIG. 6. (a) Macroion charge Z_0^c vs macroion size σ_0^c in the Belloni model determined as described in the flow chart of Fig. 3 for screening parameters $\mathbf{k}=3$ (circles) and $\mathbf{k}=6$ (triangles). (b) Same as (a) but for the DLVO model.

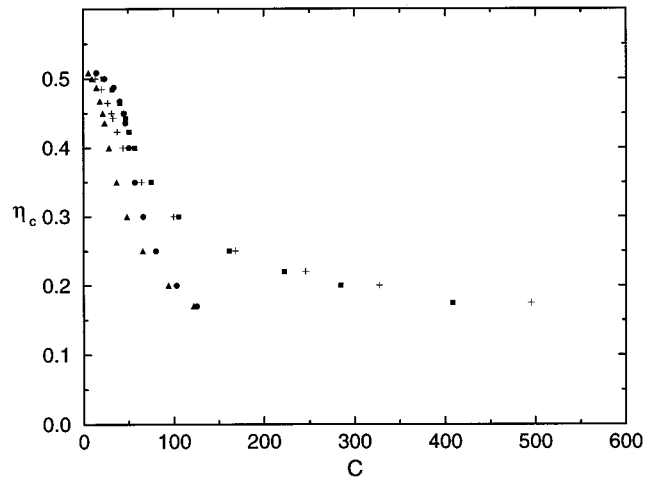

FIG. 7. Volume fraction η_c vs electrostatic potential $\mathbf{C}$, which is $\mathbf{C}=Z_0^{c2}/\sigma_0^c$ for Belloni or $\mathbf{C}=\overline{Z_0^{c2}}/\sigma_0^c$ for DLVO at $\mathbf{k}=3$ in the Belloni (triangles) and the DLVO (circles) models compared with those at $\mathbf{k}=6$ in the Belloni (plusses) and the DLVO (squares) models.

theless, it is interesting to remark that for both weak screening cases in Fig. 5(c), as η decreases to lower values the role of intermediate- and long-ranged interactions manifests, and structural changes are now characterized by the relative importance of these latter two factors. This accounts for the general tendency of merging for the set of η_c-Z_0^c and η_c-$\overline{Z_0^c}$ curves at $\mathbf{k}=3$ as η decreases. Turning to the case $\mathbf{k}=6$ [Fig. 5(d)], here we have relatively many small ions surrounded the macroparticles, and the effective screening effect will tend to reduce the subtle role of Z_0^c, making its contribution to structure inconsequential. One would therefore expect qualitatively similar structures for the Belloini and DLVO models with finer details being quantitatively embellished by the η dependence of X.

Coming to the second aspect, this can be explained as follows. For the case $\mathbf{k}=3$ the ionic screening effect leads to a relatively stronger electrostatic force and this would imply a larger macroion charge (and hence a longer interaction range), which then acts to degrade the role of geometric hard core. For a given surface charge parameter γ, the σ_0 must increase enormously at a constant Λ, which must be so since the latter physically accounts for the macroion-ion correlations. This, however, is in opposition to the case $\mathbf{k}=6$ where the comparatively larger effective screening effect has considerably weakened the Coulomb repulsions (and hence Z_0^c or $\overline{Z_0^c}$) between macroparticles and the σ_0 increases less wildly. It should be emphasized that such a change in σ_0 is to rectify the inconsistency of the OCM for the inverse screening length κ and should not be confused with the rescaling idea proposed by Hayter and Hansen [33] for handling the dilute dispersion of colloids at strong electrostatic coupling. The former leads to a real physical size of a macroparticle whose value was adjusted even at high η while the latter describes a macroparticle surrounded by an impenetrable volume.

IV. CONCLUSION

The structures of concentrated charge-stabilized colloidal dispersions were investigated using the OCM in the mean spherical approximation. Within the idealized mode-coupling theory, the loci of the liquid-glass transition phase boundaries were determined. It was found that for $\eta_c \lesssim 0.43$ and for strong Coulomb coupling the $g(r)$ at contact distance in the MSA becomes unphysical and needs to be rescaled. Both the $S(q)$ with and without rescaling were compared to manifest the inadequacy of the MSA closure in the specific region of parametric phase space. In attempting to explore the usefulness of the OCM, we notice an apparent inconsistency in that the Debye-Hückel screening constant κ that is defined parametrically in OCM generally differs from that defined in the primitive model in terms of physical parameters. In other words, for a given macroion size, the κ employed in the OCM calculation may be physically unrealistic. Removal of the latter inconsistency has led us to an ergodic-nonergodic phase diagram corresponding to macroions of different size and charge distribution. Finally, we compare generally the widely used DLVO model and the more refined model of Belloni. We judge from our calculated phase diagrams that the OCM of Belloni is physically sound and appropriate for extensive studies of charged colloidal structures and, within the mode-coupling theory, of the dynamics of high density colloids.

ACKNOWLEDGMENTS

We gratefully acknowledge financial support from the National Science Council of Taiwan, R.O.C. under Grant No. NSC87-2112-M-008-004 and the Australian Academy of Science with the National Science Council of Taiwan, R.O.C. for an exchange program under which the final stage of this work was completed. We also thank the National Center for High-Performance Computing of Taiwan, R.O.C. for granting special computing resources. S.K.L. would like to thank the Department of Applied Physics, Royal Melbourne Institute of Technology, Melbourne, Australia, particularly Professor W. van Megen and Professor I. K Snook, for their kind hospitality during the entire period of his stay.

APPENDIX

In this Appendix, we derive the effective direct correlation function $c_{00}^{\rm eff}(r)$ by the method of convolution. We begin with the convolution of functions $u(\mathbf{r})$ and $v(\mathbf{r})$ defined by

$$G(u\circ v)=\int v(\boldsymbol{\xi})u(\mathbf{r}-\boldsymbol{\xi})d\boldsymbol{\xi}. \tag{A1}$$

For the problem at hand, $c_{00}^{\rm eff}(r)=G^{-1}[c_{00}^{\text{generally eff}}(q)]$ for $r>\sigma_0$, which can be obtained using the formula

$$\frac{1}{\rho_0}\,G^{-1}\left(\frac{1}{q^2+\kappa^2}\right)=\Theta(r)=\frac{1}{4\pi\rho_0}\,\frac{e^{-\kappa r}}{r}, \tag{A2}$$

defining $W_1(r)=\alpha_0^2\Theta(r)$, $W_2(r)=2\alpha_0\alpha_i\Theta(r)$, and $W_3(r)=\alpha_i\alpha_j\Theta(r)$, and recalling that $c_{00}(r)=c_{0i}^s(r)=0$ for $r>\sigma_0$. Accordingly an expression for $c_{00}^{\rm eff}(r)$ can be derived

$$\begin{aligned}c_{00}^{\rm eff}(r)=&\,W_1(r)+(\rho_0\rho_i)^{1/2}W_2\circ c_{0i}^s\\&+(\rho_0\rho_i)^{1/2}W_3\circ\{(\rho_0\rho_i)^{1/2}[c_{0i}^s\circ c_{0j}^s]\}\end{aligned} \tag{A3}$$

provided the convolutions $C=G[c_{0i}^s\circ c_{0j}^s]$, $G[W_2\circ c_{0i}^s]$ and $G(W_3\circ C)$ can be determined. To calculate these we note that

$$\begin{aligned}C=&\,2\pi\int_{\xi_m}^{\xi_M}\int_{\theta_m(\xi,r)}^{\theta_M(\xi,r)}c_{0i}^s(\xi)c_{0j}^s(\theta)\,\frac{\xi\theta}{r}\,d\xi d\theta\\
=&\,2\pi\int_{\xi_m=r-a}^{\xi_M=a}\int_{\theta_m=r-\xi}^{\theta_M=a}\left(c_i+\frac{\tilde Z_i}{\xi}\right)\left(c_j+\frac{\tilde Z_j}{\theta}\right)\frac{\xi\theta}{r}\,d\xi\,d\theta\\
&+2\pi\left(\int_{\xi_m=r}^{\xi_M=a}\int_{\theta_m=\xi-r}^{\theta_M=a}+\int_{\xi_m=a-r}^{\xi_M=r}\int_{\theta_m=r-\xi}^{\theta_M=a}\right.\\
&\left.+\int_{\xi_m=0}^{\xi_M=a-r}\int_{\theta_m=r-\xi}^{\theta_M=r+\xi}\right)\left(c_i+\frac{\tilde Z_i}{\xi}\right)\left(c_j+\frac{\tilde Z_j}{\theta}\right)\frac{\xi\theta}{r}\,d\xi\,d\theta\\
&+2\pi\left(\int_{\xi_m=a-r}^{\xi_M=a}\int_{\theta_m=\xi-r}^{\theta_M=a}+\int_{\xi_m=r}^{\xi_M=a-r}\int_{\theta_m=\xi-r}^{\theta_M=\xi+r}\right.\\
&\left.+\int_{\xi_m=0}^{\xi_M=r}\int_{\theta_m=r-\xi}^{\theta_M=\xi+r}\right)\left(c_i+\frac{\tilde Z_i}{\xi}\right)\left(c_j+\frac{\tilde Z_j}{\theta}\right)\frac{\xi\theta}{r}\,d\xi\;\,d\theta,\end{aligned} \tag{A4}$$

where $\tilde Z_i=Z_0Z_iL_B$; $c_i=1/(\eta-1)-\nu\tilde Z_i/a$ [41]; ξ_M, ξ_m, θ_M, and θ_m are the limits of integration variables subject to the constraint $r>\sigma_0$. Similarly

$$\begin{aligned}G[W_2\circ c_{0i}^s]=&\,2\pi\int_{\xi_m=0}^{\xi_M=a}\int_{\theta_m=r-\xi}^{\theta_M=r+\xi}\\&\times\frac{e^{-\kappa r}}{r}\left(c_i+\frac{\tilde Z_i}{\xi}\right)\frac{\xi\theta}{r}\,d\xi\,d\theta,\end{aligned}$$

and $G(W_3\circ C)$ is obtained by convoluting Eqs. (A2) and (A4).

[1] P. N. Pusey and W. van Megen, Nature (London) **320**, 340 (1986).
[2] Y. Yang and K. A. Nelson, Phys. Rev. Lett. **74**, 4883 (1995).
[3] J. Wuttke, M. Kiebel, E. Bartsch, F. Fujara, W. Petry, and H. Sillescu, Z. Phys. B **91**, 357 (1993).
[4] X. C. Zeng, D. Kivelson, and G. Tarjus, Phys. Rev. Lett. **72**, 1772 (1994); W. van Megen and S. M. Underwood, *ibid.* **72**, 1773 (1994); X. C. Zeng and D. Kivelson, Phys. Rev. E **50**, 1711 (1994); H. Z. Cummins and G. Li, *ibid.* **50**, 1720 (1994).
[5] U. Bengtzelius, W. Götze, and A. Sjölander, J. Phys. C **17**, 5915 (1984).
[6] R. Schmitz, J. W. Dufty, and P. De, Phys. Rev. Lett. **71**, 2066 (1993).
[7] J. Yeo, Phys. Rev. E **52**, 853 (1995).
[8] T. Odagaki, Phys. Rev. Lett. **75**, 3701 (1995).
[9] W. Götze, in *Liquids, Freezing and the Glass Transition*, edited by J. P. Hansen, D. Levesque, and J. Zinn-Justin (North-Holland, Amsterdam, 1991), p. 287; W. Götze and L. Sjögren, Rep. Prog. Phys. **55**, 241 (1992).
[10] J. L. Barrat, W. Götze, and L. Latz, J. Phys.: Condens. Matter **1**, 7163 (1989).
[11] M. Fuchs, I. Hofacker, and A. Latz, Phys. Rev. A **45**, 898 (1992).
[12] S. K. Lai and S. Y. Chang, Phys. Rev. B **51**, R12869 (1995).
[13] U. Bengtzelius, Phys. Rev. A **34**, 5059 (1986).
[14] W. J. Ma and S. K. Lai, Physica B **233**, 221 (1997).
[15] S. K. Lai and H. C. Chen, J. Phys.: Condens. Matter **5**, 4325 (1993).
[16] S. K. Lai and H. C. Chen, J. Phys.: Condens. Matter **7**, 1499 (1995).
[17] H. C. Chen and S. K. Lai, Phys. Rev. E **56**, 4381 (1997).
[18] J. Bosse and J. S. Thakur, Phys. Rev. Lett. **59**, 998 (1987); Phys. Rev. A **43**, 4378 (1991); **43**, 4388 (1991).
[19] W. Kob and H. C. Andersen, Phys. Rev. Lett. **73**, 1376 (1994).
[20] Y. Kaneko and J. Bosse, J. Phys.: Condens. Matter **8**, 9581 (1996).
[21] W. J. Ma and S. K. Lai, Phys. Rev. E **55**, 2026 (1997).
[22] S. Kämmerer, W. Kob, and R. Schilling, Phys. Rev. E **56**, 5450 (1997).
[23] T. Franosch, M. Fuchs, W. Gotze, M. R. Mayr, and A. P. Singh, Phys. Rev. E **56**, 5659 (1997).

[24] S. K. Lai, W. J. Ma, W. van Megen, and I. K. Snook, Phys. Rev. E **56**, 766 (1997). A preliminary study of the liquid-glass transition phase diagram within the DLVO potential (see text) was given in this work. Equations (2)–(4) given there should respectively be replaced more correctly by Eqs. (21)–(23) here. The latter equations are appropriate for a colloidal suspension. These changes, however, do not affect the numerical values for the idealized liquid-glass transition loci since the solidification equation remains unchanged (rigorous justification is given in Refs. [25], [27], and [28]).
[25] G. Szamel and H. Löwen, Phys. Rev. A **44**, 8215 (1991).
[26] B. Cichocki and W. Hess, Physica A **141**, 475 (1987).
[27] P. Baur, G. Nägele, and R. Klein, Phys. Rev. E **53**, 6224 (1996); Physica A **245**, 297 (1997).
[28] K. Kawasaki, Physica A **208**, 35 (1994); Butsuri, Bull., Phys. Soc. Jpn.) **48**, 869 (1993) (in Japanese).
[29] E. J. Verwey and J. G. Overbeek, *Theory of the Stability of Lyophobic Colloids* (Elsevier, Amsterdam, 1948).
[30] M. J. Grimson and M. Silbert, Mol. Phys. **74**, 397 (1991).
[31] H. Löwen, J. P. Hansen, and P. A. Madden, J. Chem. Phys. **98**, 3275 (1993).
[32] J. B. Hayter and J. Penfold, Mol. Phys. **42**, 109 (1981).
[33] J. P. Hansen and J. B. Hayter, Mol. Phys. **46**, 651 (1982).
[34] J. B. Hayter, J. Chem. Soc., Faraday Trans. **77**, 1851 (1981); Faraday Discuss. Chem. Soc. **76**, 7 (1983).
[35] M. Medina-Noyola and D. A. McQuarrie, J. Chem. Phys. **73**, 6279 (1980).
[36] M. Medina-Noyola, J. Chem. Phys. **77**, 1428 (1982).
[37] B. Beresford-Smith and D. Y. C. Chan, Chem. Phys. Lett. **92**, 474 (1982).
[38] B. Beresford-Smith, D. Y. C. Chan, and D. J. Mitchell, J. Colloid Interface Sci. **105**, 216 (1985).
[39] S. A. Adelman, Chem. Phys. Lett. **38**, 567 (1976); J. Chem. Phys. **64**, 724 (1976).
[40] L. Belloni, J. Chem. Phys. **85**, 519 (1986).
[41] K. Hiroike, J. Phys. Soc. Jpn. **27**, 1415 (1969); Mol. Phys. **33**, 1195 (1977).
[42] S. H. Chen, E. Y. Sheu, J. Kalus, and H. Hoffmann, J. Appl. Crystallogr. **21**, 751 (1988).
[43] H. Ruiz-Estrada, M. Medina-Noyola, and G. Nägele, Physica A **168**, 919 (1990).
[44] S. Khan, T. L. Morton, and D. Ronis, Phys. Rev. A **35**, 4295 (1987).
[45] G. Nägele, R. Klein, and M. Medina-Noyola, J. Chem. Phys. **83**, 2560 (1980).
[46] G. Senatore and L. Blum, J. Phys. Chem. **89**, 2676 (1985).
[47] P. Linse, J. Chem. Phys. **94**, 3817 (1991).
[48] M. Ginoza, J. Phys. Soc. Jpn. **55**, 95 (1986).
[49] E. Arrieta, C. Jedrzejec, and K. N. March, J. Chem. Phys. **86**, 3607 (1986).
[50] G. Pastore, Mol. Phys. **63**, 731 (1988).
[51] D. Ronis, J. Chem. Phys. **81**, 2749 (1984).
[52] Y. V. Kalyuzhnyi, L. Blum, M. F. Holovko, and I. A. Protsykevytch, Physica A **236**, 85 (1997).
[53] Here we follow the work of [27] for the definition of the memory function, which differs from those of [26,25] by a factor D_0q^2 [cf. Eq. (1.2) in [26] and Eq. (13) in [27]].
[54] L. Sjögren, Phys. Rev. A **22**, 2883 (1980).
[55] U. Bengtzelius, Phys. Rev. A **33**, 3433 (1986).
[56] E. Y. Sheu, C. F. Wu, and S. H. Chen, Phys. Rev. A **32**, 3807 (1985).
[57] L. Belloni, J. Chem. Phys. **88**, 5143 (1988).
[58] G. Senatore, in *Structure and dynamics of Strongly Interacting Colloids and Supramolecular Aggregates in Solution*, edited by S. H. Chen, J. S. Huang, and P. Tartaglia (Kluwer Academic, Dordrecht, 1992), p. 181.
[59] K. S. Schmitz, *Macroions in Solution and Colloidal Suspension* (VCH, New York, 1993), pp. 17–67.